Physics in Medicine & Biology

PAPER

Novel inter-crystal scattering event identification method for PET detectors

To cite this article: Min Sun Lee *et al* 2018 *Phys. Med. Biol.* **63** 115015

IOP Publishing Phys. Med. Biol. 63 (2018) 115015 (13pp) https://doi.org/10.1088/1361-6560/aabe3a

Physics in Medicine & Biology

IPEM Institute of Physics and Engineering in Medicine

CrossMark

RECEIVED
27 December 2017

REVISED
27 March 2018

ACCEPTED FOR PUBLICATION
16 April 2018

PUBLISHED
7 June 2018

PAPER

Novel inter-crystal scattering event identification method for PET detectors

Min Sun Lee[1,2], Seung Kwan Kang[2,3] and Jae Sung Lee[1,2,3]

1 Interdisciplinary Program in Radiation Applied Life Science, Seoul National University, Seoul 03080, Republic of Korea
2 Department of Nuclear Medicine, College of Medicine, Seoul National University, Seoul 03080, Republic of Korea
3 Department of Biomedical Sciences, College of Medicine, Seoul National University, Seoul 03080, Republic of Korea

E-mail: jaes@snu.ac.kr

Keywords: inter-crystal scattering, positron emission tomography, PET detector, convex constrained optimization

Abstract

Here, we propose a novel method to identify inter-crystal scattering (ICS) events from a PET detector that is even applicable to light-sharing designs. In the proposed method, the detector observation was considered as a linear problem and ICS events were identified by solving this problem. Two ICS identification methods were suggested for solving the linear problem, pseudoinverse matrix calculation and convex constrained optimization. The proposed method was evaluated based on simulation and experimental studies. For the simulation study, an 8×8 photo sensor was coupled to 8×8, 10×10 and 12×12 crystal arrays to simulate a one-to-one coupling and two light-sharing detectors, respectively. The identification rate, the rate that the identified ICS events correctly include the true first interaction position and the energy linearity were evaluated for the proposed ICS identification methods. For the experimental study, a digital silicon photomultiplier was coupled with 8×8 and 10×10 arrays of $3 \times 3 \times 20$ mm^3 LGSO crystals to construct the one-to-one coupling and light-sharing detectors, respectively. Intrinsic spatial resolutions were measured for two detector types. The proposed ICS identification methods were implemented, and intrinsic resolutions were compared with and without ICS recovery. As a result, the simulation study showed that the proposed convex optimization method yielded robust energy estimation and high ICS identification rates of 0.93 and 0.87 for the one-to-one and light-sharing detectors, respectively. The experimental study showed a resolution improvement after recovering the identified ICS events into the first interaction position. The average intrinsic spatial resolutions for the one-to-one and light-sharing detector were 1.95 and 2.25 mm in the FWHM without ICS recovery, respectively. These values improved to 1.72 and 1.83 mm after ICS recovery, respectively. In conclusion, our proposed method showed good ICS identification in both one-to-one coupling and light-sharing detectors. We experimentally validated that the ICS recovery based on the proposed identification method led to an improved resolution.

1. Introduction

Positron emission tomography (PET) is an essential imaging device which provides diagnostic information in a wide range of disease states (Phelps 2000, Kim 2016, Ahn 2017). PET provides tomographic images by detecting a pair of 511 keV annihilation gamma rays generated from the radiopharmaceuticals distributed in a patient's body. When a 511 keV gamma ray enters a PET detector, the gamma ray deposits its energy by undergoing photoelectric (PE) absorption or Compton scattering within a PET detector. For the latter case, the scattered photon and emitted photoelectron deposits a portion of their energy in more than one crystal element, and this phenomenon is referred to as an inter-crystal scattering (ICS) event. ICS events cause the mis-positioning of gamma interaction, resulting in false lines-of-response (LOR). These false LOR lead to a degraded image resolution and contrast (Surti and Karp 2018). Since the 511 keV gamma used in PET has a large cross-section in Compton scattering, ICS is a common phenomenon in PET systems (Comanor *et al* 1996). The occurrence of ICS increases in high-resolution applications with narrower crystal elements (Shao *et al* 1996). Moreover, the occurrence of ICS depends on the linear attenuation coefficient of scintillation materials, as well as detector and system geometries. Based on our simulation study, approximately 35% of events detected within the 350–650 keV energy window undergo ICS in a PET detector with a 10×10 array of $3 \times 3 \times 20\,\text{mm}^3$ LSO crystals. Hence, the resolution degradation can be minimized and the system sensitivity can be maximized by identifying the interaction positions and deposited energies of the ICS event and recovering it into the true first interaction position.

To identify ICS events, the individual signal readout from a one-to-one coupled crystal and photo sensor pixel is considered as a feasible method, as shown in figure 1(a) (Rafecas *et al* 2003, Pratx and Levin 2009). However, the one-to-one coupling design has limitations in terms of high-resolution applications. In particular, in the case of using a silicon photomultiplier (SiPM) as a photo sensor, it is technically challenging to produce multi-pixel photo sensors with small pixel sizes while avoiding performance degradation (e.g. energy linearity, packing fraction, etc) (Roncali and Cherry 2011). Therefore, most current PET detectors use a light-sharing design by coupling multiple crystal elements with multiple photo sensor pixels as shown in figure 1(b) (Levin and Zaidi 2007). However, it is hard to identify ICS events in light-sharing PET detectors, because the light outputs from two or more crystal elements are shared by multiple photosensor pixels. Image reconstruction with a point spread function (PSF) modeling technique is an alternative solution for mitigating resolution degradation by including ICS in the model (Alessio *et al* 2006, Panin *et al* 2006). However, this approach does not realize event-by-event ICS correction and some image artifacts (e.g. edge artifacts) were observed (Rahmim *et al* 2013).

Recovering the ICS event into the first interaction position is important as well as identifying the ICS interaction positions and energies. Several groups have previously investigated techniques to choose the first interaction position. Examples include choosing the interaction position with the maximum or second maximum energy deposition (Comanor *et al* 1996, Shao *et al* 1996, Surti and Karp 2018) and choosing the interaction position that satisfies the Compton kinematics (Rafecas *et al* 2003). Gross-Weege *et al* (2016) proposed a maximum-likelihood-based positioning algorithm to identify the first interaction position by using the measured light distribution and the corresponding probability density functions. Lage *et al* (2015) suggested a proportional method for recovering inter-detector scattering events, which distributes multiple coincidence events among their possible LOR using the relative proportions of double coincidences in the corresponding ones. The proportional method is presented in equation (8), and Lage *et al* (2015) has analytically shown that this equation (8) is a maximum-likelihood solution.

In this study, we propose a new method to classify and identify ICS events from a PET detector. We consider detector observation to be a linear problem, and ICS events were identified by solving this problem. The proposed method is applicable in light-sharing designs, even with a multiplexing readout scheme, which is something that has not been suggested or developed in the publications. In this study, we investigated the proposed ICS identification method based on Monte Carlo simulation and experimental studies. Based on this new ICS identification method, ICS event positions and energies were identified and used to determine the first interaction position in order to see the impact of ICS correction.

2. Materials and methods

2.1. ICS event identification

2.1.1. Proposed algorithm

Suppose a PET detector consisted of n scintillation crystal elements coupled to m photo sensor pixels as in figure 1. Let us consider that PE absorption occurs in a detector and a 511 keV gamma ray fully deposits its energy in a single crystal as shown in figure 1. Here, we define the observation of a single PE event as a vector ($\boldsymbol{y}$), which consists of m detector responses (photo sensor pixel values) as in equation (1).

$$\boldsymbol{y} = [y_1, \ldots, y_m]^{\mathrm{T}}. \tag{1}$$

Consider that an ICS event occurs at the ith and jth crystals ($i, j \in n$) while depositing energies of E_i and E_j ($E_{total} = E_i + E_j$), as shown in figure 1. Then, the observation $\boldsymbol{y}$ of an ICS event can be expressed as the sum of independent observations of $\boldsymbol{y_i}$ and $\boldsymbol{y_j}$ multiplied by the corresponding energy ratios as shown in equation (2). In equation(2), $\boldsymbol{y_i}$ and $\boldsymbol{y_j}$ are independent detector observations when PE absorption occurs at the ith and jth crystals, respectively. Here, we assume that ICS events (multiple hit events) can be expressed as the superposition of independent PE events (single hit events)

$$\boldsymbol{y} = \boldsymbol{y_i} \times E_i/E_{total} + \boldsymbol{y_j} \times E_j/E_{total}. \tag{2}$$

Equation (2) can be simply converted into a matrix formation

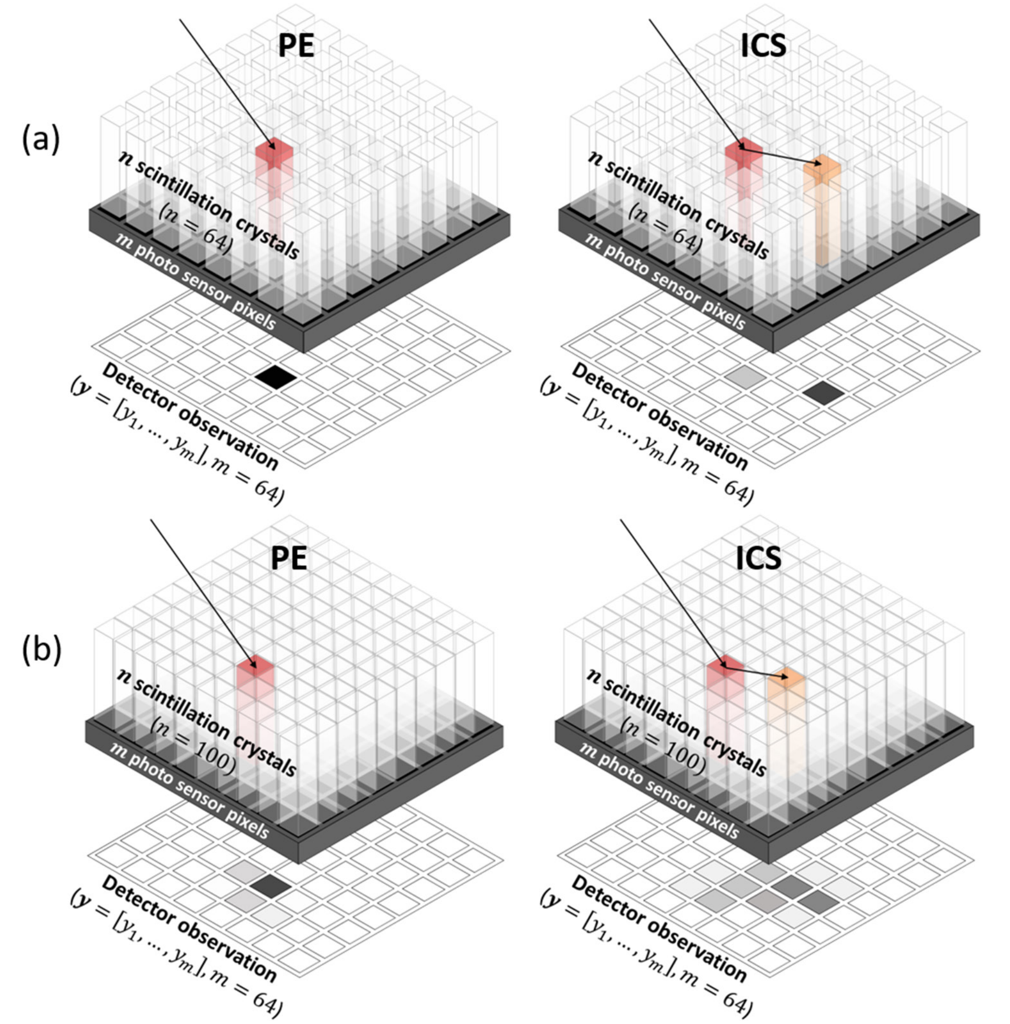

Figure 1. PET detectors consisting of n scintillation crystals and m photo sensor pixels and the observed detector responses (photo sensor pixel values). (a) In the one-to-one coupling design, crystals ($n = 64$) were individually coupled to the photo sensor pixels ($m = 64$). (b) In the light-sharing design, 10×10 arrays of crystals ($n = 100$) were coupled to 8×8 photo sensor pixels ($m = 64$).

$$\boldsymbol{y} = \boldsymbol{A}\boldsymbol{x}; \quad \begin{bmatrix} y_1 \\ \vdots \\ y_m \end{bmatrix} = \begin{bmatrix} a_{1,1} & \cdots & a_{1,n} \\ \vdots & \ddots & \vdots \\ a_{m,1} & \cdots & a_{m,n} \end{bmatrix} \times \begin{bmatrix} x_1 \\ \vdots \\ x_n \end{bmatrix}, \tag{3}$$

where $\boldsymbol{y}$ is an m-dimensional vector of a single ICS event observation, $\boldsymbol{A}$ is an $[m \times n]$ matrix of m characteristic detector responses for n crystals, and $\boldsymbol{x}$ is an n-dimensional vector containing the energy ratios for n crystals. The vector $\boldsymbol{y}$ is a measured value from the detector response from a single gamma event. The matrix $\boldsymbol{A}$ is also a measured value that can be generated from detector data sets by calculating the mean detector responses for each crystal position. Consequently, finding vector $\boldsymbol{x}$, which represents the deposited energy ratios at n crystal elements of a single gamma event, we can identify the ICS event positions and corresponding deposited energies.

To find $\boldsymbol{x}$, we compared three different ICS identification methods:

(1) Method 1: maximum peak detection

$$\max(\boldsymbol{y}) \tag{4}$$

(2) Method 2: pseudoinverse matrix calculation

$$\boldsymbol{x} = \left(\boldsymbol{A}^T\boldsymbol{A}\right)^{-1}\boldsymbol{A}^{\mathrm{T}}\boldsymbol{y}. \tag{5}$$

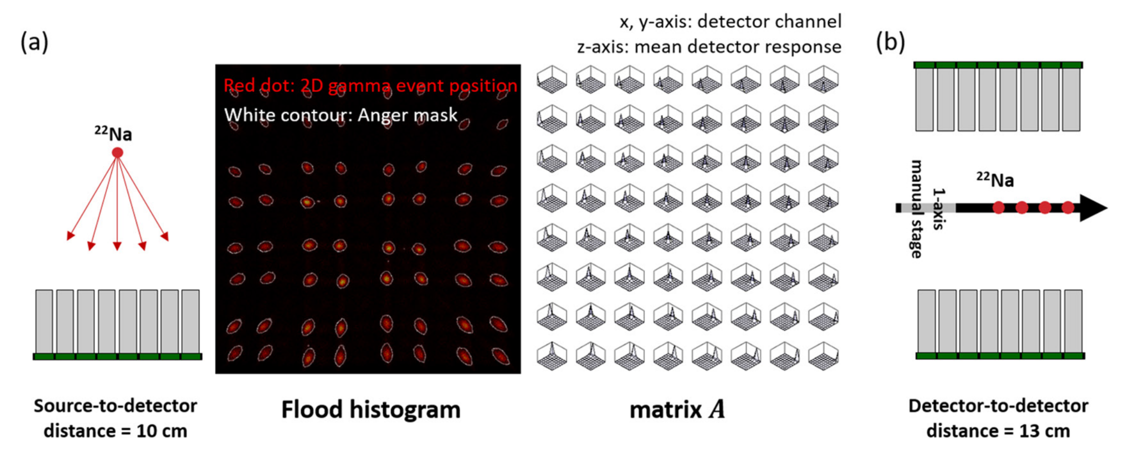

Figure 2. (a) Matrix $\boldsymbol{A}$ calculation. From the detector irradiated with a point source, a flood histogram (red dots) was acquired. An anger mask was applied to the flood histogram, which is represented by the white contour. The detector responses of each crystal position were extracted, and the mean detector responses of each crystal position were calculated consequently. (b) The experimental setup for the intrinsic spatial measurement.

(3) Method 3: convex constrained optimization

$$\begin{aligned} &\arg\min_{\boldsymbol{x}} \|\boldsymbol{y} - \boldsymbol{A}\boldsymbol{x}\|_2 \\ &\text{subject to} \quad \boldsymbol{x} > 0, \\ &\qquad\qquad \sum \boldsymbol{x} = 1. \end{aligned} \tag{6}$$

Method 1 is a typical approach used in a one-to-one coupling detector with an individual signal readout and identifies the ICS events by finding maximum values from the observation ($\boldsymbol{y}$). Method 1 was tested as a reference. Methods 2 and 3 are the ICS identification methods proposed in this study which identify the ICS event from the energy ratio vector ($\boldsymbol{x}$). Method 2 simply calculates a pseudoinverse matrix to solve the linear problem in equation (5). However, a pseudoinverse can result in negative entries in $\boldsymbol{x}$. Hence, method 3 is proposed to solve the linear problem with the constraints given in equation (6). The solution was found using convex constrained optimization. To solve the convex optimization problem, a Matlab-based CVX program (Grant and Boyd 2011) was used.

2.1.2. Event classification and identification

As the first step of event classification and identification, matrix $\boldsymbol{A}$ was calculated as described in figure 2(a). A flood histogram (a 2D histogram of the gamma interaction positions) was generated by calculating the energy-weighted mean of the pixel values from the listmode detector dataset. Since most of ICS events are distributed in between the crystals in the flood histogram, an anger mask is applied to the flood histogram to reject ICS events (Ling *et al* 2007). From the masked flood histogram, the detector responses of the n crystals were extracted. Matrix $\boldsymbol{A}$ was then generated by calculating the average of the m detector responses at each crystal position.

Based on observation $\boldsymbol{y}$ and the calculated matrix $\boldsymbol{A}$, we can find vector $\boldsymbol{x}$ by using three different identification methods, as explained in section 2.1.1. Events were classified into two event types of PE absorption and ICS events based on the energy ratio vector $\boldsymbol{x}$. Each event type was classified according to the following criteria, while the constant c was determined based on the simulation.

(1) PE events: $\frac{\max(\boldsymbol{x})}{\text{second } \max(x)} > c$
(2) ICS events: $\frac{\max(\boldsymbol{x})}{\text{second} \max(\boldsymbol{x})} \leqslant c$

The interaction positions and deposited energies of classified ICS events were identified by using indices and values of the energy ratio vector $\boldsymbol{x}$. Considering the case where an ICS event occurs only once, the indices of the two maximum values in $\boldsymbol{x}$ were determined to be the interacting crystal positions, while the values of $\boldsymbol{x}$ were determined to be the deposited energy ratios. Figure 3 shows the energy ratio vector $\boldsymbol{x}$ of the typical PE and ICS events acquired from convex optimization.

The 'identification rate' was calculated using equation (7) to evaluate the performance of the methods, that is to say, the number of identified ICS events that include the true first interaction position divided by the total number of ICS events. The energy linearity and correlation were also evaluated by conducting a linear fit between the true energy values and estimated energies.

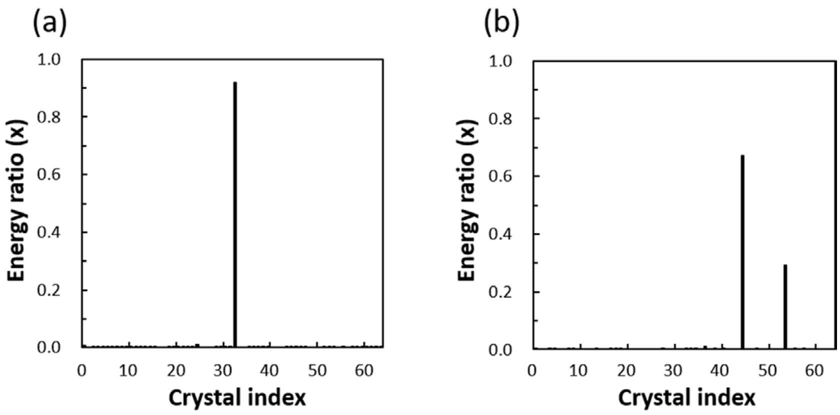

Figure 3. The energy ratio vectors ($\boldsymbol{x}$) of the one-to-one coupling detector, which represent the deposited energy ratios at 8 × 8 crystal positions for the representative (a) PE absorption and (b) ICS events.

$$\text{Identification rate} = \frac{\#\text{ of ICS events including the true first interaction position}}{\#\text{ of total ICS events}}. \tag{7}$$

2.2. Simulation study

2.2.1. GATE Monte Carlo simulation setup

To evaluate the proposed methods, a simulation study was conducted using a GATE v.7.0 Monte Carlo simulation toolkit with optical photon tracking (Jan *et al* 2004, 2011). In the simulation, the medium surfaces and interactions at the medium boundaries were simulated based on the UNIFIED model (Levin and Moisan 1996). In the UNIFIED model, the surface is composed of small micro-facets. The surfaces were defined by specifying the standard deviation (sigma-alpha) of the Gaussian distribution of the micro-facets around the average surface normal. The interactions at the boundaries are simulated based on the micro-facet orientations and refractive indices.

The simulated detector consists of arrays of polished LSO (Lu_2SiO_5; $d = 7.5$ g cm^{-3}; refractive index 1.82) crystals. While the typical LSO has a light yield of 26 000 photons MeV^{-1}, here, we assigned the light yield to be 10 400 photons MeV^{-1} by considering a 40% photo sensor photon detection efficiency (PDE)of the photo sensor used in this study. LSO crystals were wrapped with specular reflectors with 98% reflectivity, and all the gaps between the crystals were filled with air. All the polished crystal surfaces were set to a sigma-alpha value of 0.1.

The photo sensor was simulated to have the same geometry as a digital silicon photomultiplier (dSiPM; Philips Digital Photon Counting, Aachen, Germany). The diSiPM consists of 8 × 8 pixels, and each pixel has a dimension of 3.2 × 3.8775 mm^2. The pixel array was covered with a 0.1 mm thick glass entrance ($d = 2.5$ g cm^{-3}; refractive index 1.5). The photo sensor and crystal array were optically coupled with a 0.1 mm thick optical grease ($d = 1.0$ g cm^{-3}; refractive index 1.465). The sigma-alpha value was set to 0.0 for the pixel and 0.1 for the glass entrance and optical grease surfaces. All optical photons entering the pixel were detected with 100% efficiency. Here, we did not incorporate any SiPM sensitivity variations or noise properties.

For the simulation study, three detector configurations with different crystal-to-sensor coupling ratios were used, as shown in table 1. The crystal-to-sensor coupling ratio defined here corresponds to the ratio of the number of crystal elements to the number of photo sensor pixels.

The detector was irradiated using an isotropic 511 keV gamma point source that was located 10 cm apart from the detector. Moreover, three representative signal readout schemes were applied to the simulated 8 × 8 detector responses in order to investigate the effect of signal multiplexing on the proposed algorithm.

(1) Individual readout (1:1 signal multiplexing)
(2) Row-and-column sum (RC sum) readout (4:1 signal multiplexing)
(3) Four corner readout (16:1 signal multiplexing)

Identification rate and energy linearity performances were evaluated for the three detector configurations with different signal readout schemes by using the three identification methods. All the simulation cases were evaluated with approximately 40 000 gamma events that entered within the energy window of 350–650 keV.

2.2.2. ICS event recovery schemes

As mentioned in the introduction, recovering ICS events into the first interaction position is important as well as identifying ICS interaction positions and energies. The ICS recovery schemes were initially investigated based

Table 1. Specifications of the simulated detector configurations.

Crystal-to-sensor coupling ratio	Crystal size (mm^3)	Crystal array size
1:1	$3 \times 3 \times 20$	8×8
1.25:1	$3 \times 3 \times 20$	10×10
1.5:1	$2.5 \times 2.5 \times 20$	12×12

on simulation. From the simulation data, where the detector was irradiated with the cone beam, the ICS events were identified with the convex optimization method. The identified ICS events were then recovered using the maximum energy deposition (Shao *et al* 1996) and proportional methods (Lage *et al* 2015). The ICS recovered results were compared to the results without ICS recovery and the true first interaction values. In this study, we chose to use the proportional method, as originally suggested by Lage *et al* (2015) as in equation (8) below. In this study, we adopted the proportional method that originally recovers inter-detector scattering events in the system level and extended the method to be used to recover ICS events in the detector level.

$$\mathrm{LOR}_{i-j} = D_{i-j} + \sum_{k}^{n} \left(\frac{D_{i-j}}{D_{i-j} + D_{i-k} + D_{j-k}} \right) T_{i-j-k}. \tag{8}$$

In equation (8), $\mathrm{LOR}_{i\text{–}j}$ represents the final number of counts, including PE and ICS events along the LOR connecting the interacting crystals i and j. $D_{i\text{–}j}$, $D_{i\text{–}k}$ and $D_{j\text{–}k}$ represent the number of coincidences that underwent PE along the interaction positions i–j, i–k and j–k. $T_{i\text{–}j\text{–}k}$ is the number of coincidences that underwent ICS at positions i, j and k.

2.3. Experimental study

2.3.1. Detector and experimental setup

Experimental studies were conducted to demonstrate the feasibility of the proposed methods. The one-to-one coupling and light-sharing detectors were constructed using Philips dSiPMs coupled with $3 \times 3 \times 20\,\mathrm{mm}^3$ LGSO ($Lu_{1.9}Gd_{0.1}SiO_5$:Ce; Hitachi Chemical, Tokyo, Japan) crystal arrays. As mentioned earlier, the dSiPM consists of 8×8 pixels. For the one-to-one coupling design, 64 LGSO crystals were individually coupled to 64 dSiPM pixels. For the light-sharing design, a 10×10 LGSO crystal array with a pitch size of 3.1 mm was coupled to 64 dSiPM pixels. All the components were optically coupled using optical grease (BC-630, OKEN, Japan). Each crystal was wrapped with enhanced specular reflectors (ESR; 3M, St Paul, MN, USA) except for the face that was optically coupled to the dSiPM. The 8×8 detector responses were recorded individually using a PDPC technical evaluation kit (PDPC-TEK User Manual 2014). Post-processing was applied to demonstrate the RC sum signal multiplexing. The configurations of the dSiPM were set to trigger level four, validation level eight, an integration length of 165 ns, full neighbor logic and a 40 ns coincidence window (Lee and Lee 2015, Lee *et al* 2017).

2.3.2. Intrinsic spatial resolution measurement

An intrinsic spatial resolution measurement was conducted using a detector pair separated by a distance of 13 cm and a ^{22}Na point source located at the center, as shown in figure 2(b). By moving the point source in the axial direction with a step size of 0.5 mm from the center to the edge of the detector pair, a coincidence measurement was conducted. The counts of the opposite crystal pair for both the one-to-one and light-sharing detectors were acquired at thirty sequential source positions and represented as a count profile. The count profiles of four crystals were acquired with an energy window of 350–650 keV. The experimental set up was placed inside a temperature control box (CT-BDI150; Coretech Inc., Korea) which was set to 15 °C.

The three ICS identification methods described in section 2.1.1 were applied to the experimental data for event classification and identification. The acquired events were classified into PE and ICS events based on the classification criteria, and the interaction positions and deposited energies were identified using the three identification methods. The identified ICS events were recovered in the first interaction position using the proportional method. Gaussian fitting was applied to the ICS event to recover the count profiles of four opposing crystal pairs, and the FWHM (full width at half maximum) and FWTM (full width at tenth maximum) of each profile were calculated. Intrinsic resolutions averaged over four crystal positions were reported using the FWHM and FWTM values.

3. Results

3.1. Simulation results

3.1.1. One-to-one coupling design

Figure 4(a) shows an example of ICS identification using the convex optimization method. In the case where a single ICS event occurs once in the detector, 8×8 sensor pixel values ($\boldsymbol{y}$) were observed and represented by their

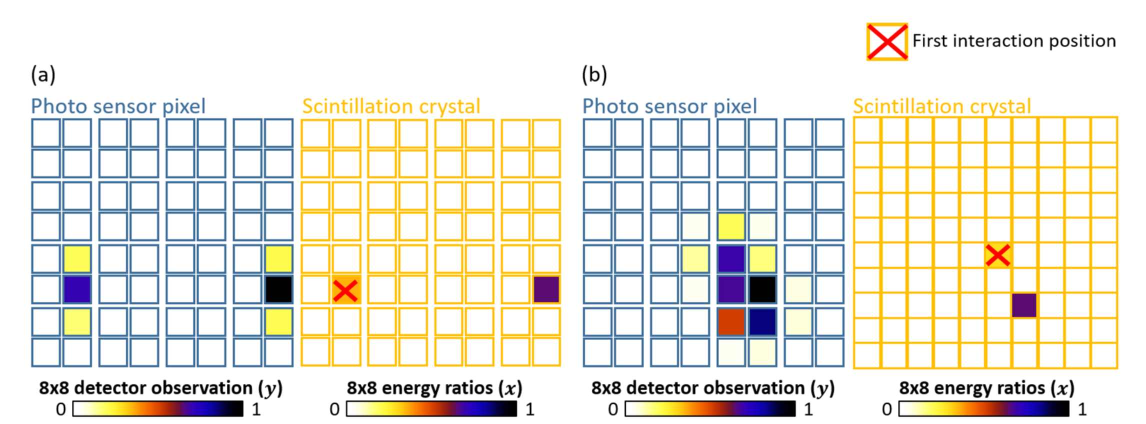

Figure 4. Examples of ICS event identification using the convex optimization method applied to (a) the one-to-one coupling detector and (b) the light-sharing detector. The blue square represents 8 $\times$ 8 photo sensor pixels, and the observations ($\boldsymbol{y}$) of a single ICS event are shown in the normalized values. The yellow square represents the crystal array coupled to the photo sensor, and the energy ratio values of each crystal ($\boldsymbol{x}$) are shown. The red '$\times$' symbol indicates the true first interaction position.

normalized values, as in figure 4(a). From the observations, we can expect two peaks might be the ICS interaction positions. Based on the proposed method, the deposited energy ratio vector $\boldsymbol{x}$ at the 8 $\times$ 8 crystal positions was acquired, and the two peak positions in $\boldsymbol{x}$ were determined to be the ICS interaction positions. By comparing the identified ICS event positions with the true first interaction position (marked with the red '$\times$' symbol), the ICS interaction positions were successfully identified using the proposed method.

The identification rate (equation (7)) and energy linearity, were investigated for the one-to-one coupling design based on the simulation study. Three different readout methods were tested, and three different identification methods were applied, as shown in table 2. With the individual signal readout (1:1 signal multiplexing), the three identification methods showed the highest identification rates. Among them, the proposed pseudoinverse and convex optimization methods showed better identification rates compared to the typical maximum peak detection approach for identifying ICS events. When we consider ICS event occurred once or twice in the detector, higher identification rates were observed that nearly reached one. Since almost 98% of the ICS events occur once or twice in a detector, ICS events occurring more than twice are ignored in this study. In the RC sum signal readout from 8 $\times$ 8 detector signals, we lose the light distribution information accuracy, and the identification rate degrades in all cases. However, the convex optimization method still shows a reasonably good identification rate of 0.72. In the case of four corner signal multiplexing, ICS events cannot be identified.

The estimated deposited energies of ICS events were fit to the true energies as shown in figure 5. The individual readout case showed good linearity and correlations with the true energy for the three identification methods (figures 5(a)–(c)). After RC sum signal multiplexing, the linearity and correlation degraded in the maximum peak detection and pseudoinverse methods (figures 5(d) and (e)). However, the convex optimization method still showed a consistent linear relationship (figure 5(f)). The four corner multiplexing case was not applicable.

3.1.2. Light-sharing design

Figure 4(b) shows another example of ICS identification using the convex optimization method when a single ICS event occurs in the light-sharing detector. In this case, we cannot easily identify where ICS events take positions based on the 8 $\times$ 8 detector observations ($\boldsymbol{y}$). By using the proposed method, the energy ratio vector $\boldsymbol{x}$ was acquired and the two peak positions in $\boldsymbol{x}$ were determined to be ICS interaction positions. By comparing the identified ICS positions with the true first interaction position, we observed that the ICS interaction positions were successfully identified in the light-sharing detector.

Table 3 shows the performance of ICS event identification for two light-sharing detectors with different crystal-to-sensor coupling ratios. The two proposed identification methods were applied, since the maximum peak detection method was not applicable in the light-sharing design. For the light-sharing detector with a 1.25:1 crystal-to-sensor coupling ratio and without signal multiplexing, we achieved a good ICS identification rate of 0.94 with the convex optimization method. The identification rate degraded with the RC sum signal readout. For the light-sharing detector with a higher crystal-to-sensor coupling ratio of 1.5:1, the ICS identification rate further degraded compared to the lower coupling ratio. Still, with the individual signal readout, we achieved a reasonably good ICS identification rate of 0.83 with the convex optimization method. For both light-sharing detectors, the pseudoinverse method did not show a good identification performance.

Table 2. The ICS identification performance of the simulated one-to-one coupling detector.

Signal readout scheme	Identification method	ICS identification rate (ICS # = 1)	ICS identification rate (ICS # ⩽ 2)
Individual	Max peak detection	0.86	0.93
	Pseudoinverse	0.93	0.98
	Convex optimization	0.93	0.98
RC sum	Max peak detection	0.60	0.61
	Pseudoinverse	0.65	0.70
	Convex optimization	0.72	0.81
Four corner	Max peak detection	Not applicable	Not applicable
	Pseudoinverse	0.02	0.03
	Convex optimization	0.02	0.03

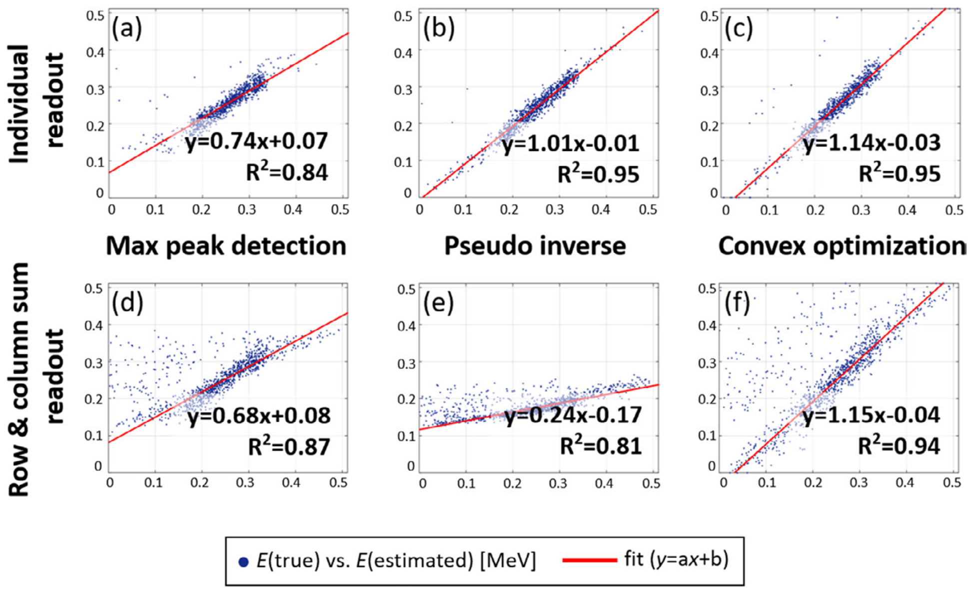

Figure 5. The energy estimation performances of the one-to-one coupling detector with an individual signal readout where ICS events were identified by (a) max peak detection, (b) pseudoinverse and (c) convex optimization. The one-to-one coupling detector with an RC sum signal readout, where the ICS events are identified by (d) max peak detection, (e) pseudoinverse and (f) convex optimization.

Table 3. The ICS identification performance of the simulated light-sharing detectors.

Crystal-to-sensor coupling ratio	Signal readout scheme	Identification method	ICS identification rate (ICS # = 1)	ICS identification rate (ICS # ⩾ 1)
1.25:1	Individual	Pseudoinverse	0.67	0.80
		Convex optimization	0.87	0.94
	RC sum	Pseudoinverse	0.53	0.62
		Convex optimization	0.65	0.73
1.5:1	Individual	Pseudoinverse	0.56	0.67
		Convex optimization	0.76	0.83
	RC sum	Pseudoinverse	0.48	0.57
		Convex optimization	0.56	0.64

The energy estimation performance of the light-sharing detectors is shown in figure 6. For all cases, the pseudoinverse method shows poor energy linearity and correlation (figures 6(a), (c), (e) and (g)). On the other hand, the convex optimization method shows consistent energy linearity and high correlation (figures 6(b) and (d)), even though there were slight degradations with the higher crystal-to-sensor coupling ratio (figures 6(f) and (h)).

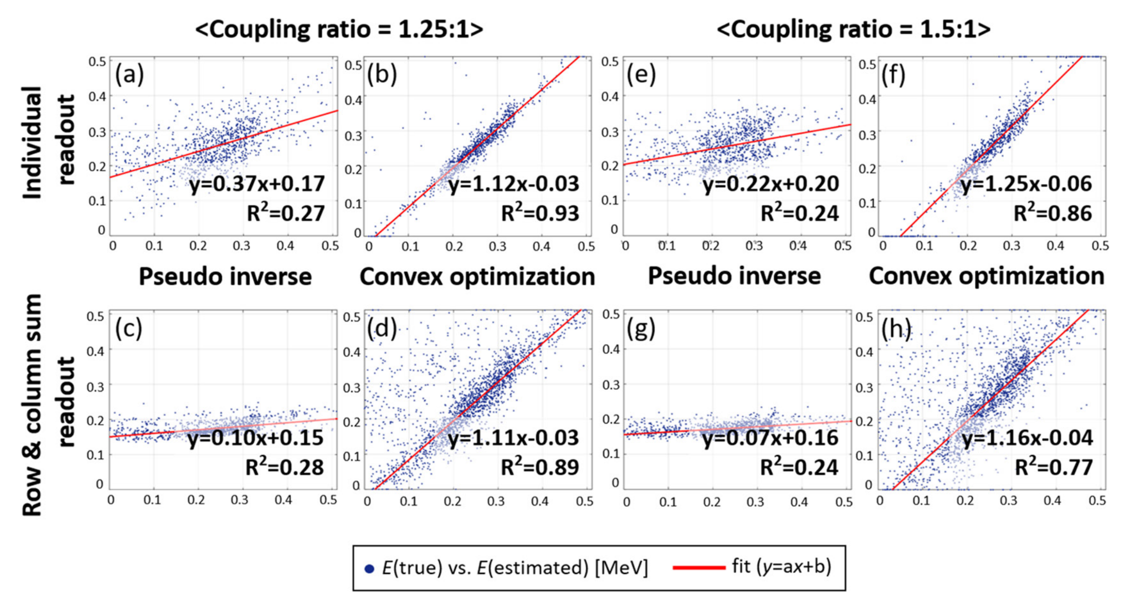

Figure 6. The energy estimation performance of the light-sharing detector with a crystal-to-sensor coupling ratio of 1.25:1 with the individual and RC sum signal readout. The ICS events identified by (a) and (c) the pseudoinverse and (b) and (d) convex optimization, respectively. The energy estimation performance of the light-sharing detector with a crystal-to-sensor coupling ratio of 1.5:1 with the individual and RC sum signal readout, where the ICS events are identified by (e) and (g) the pseudoinverse and (f) and (h) convex optimization, respectively.

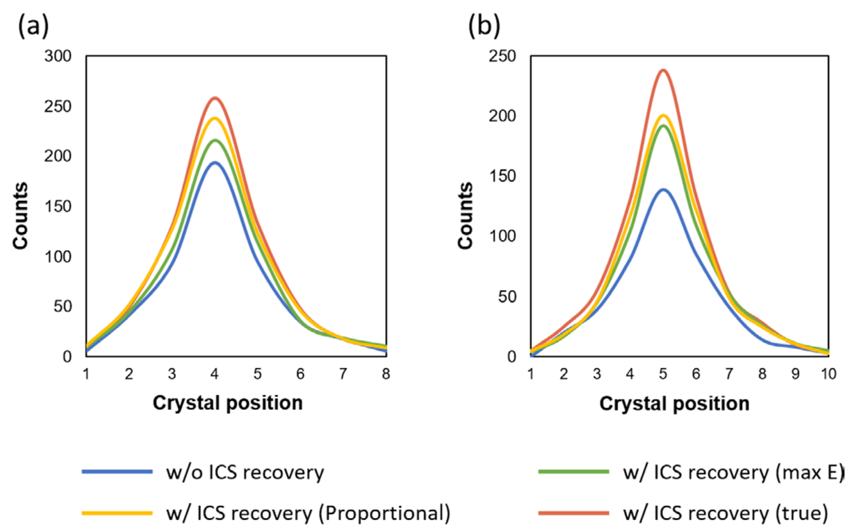

Figure 7. The count profile of (a) the one-to-one coupling detector and (b) the light-sharing detector without and with ICS recovery using maximum energy deposition and proportional methods compared to the true values.

3.1.3. ICS event recovery

ICS recovery schemes were implemented on the simulation data and compared to the true first interaction values. Figure 7 shows the count profile with and without ICS recovery for (a) one-to-one and (b) light-sharing detectors. For both detector designs, the count profiles were sharpened after ICS recovery by recovering mis-positioned LORs into the true LORs. The proportional method shows better recovery performance compared to the maximum energy deposition method, regardless of the ICS identification methods. However, the existing ICS recovery techniques could not fully recover the true interaction positions of the events, as shown in figure 7. Based on the simulation study, we decided to use the proportional method to recover the ICS events in this study.

3.2. Experimental results

3.2.1. One-to-one coupling design

As an experimental evaluation, the intrinsic spatial resolution was measured for a detector pair. The events were classified and identified using three ICS classification methods and the first interaction position was recovered using the proportional method. Events with and without ICS recovery are shown in the count profiles, as in

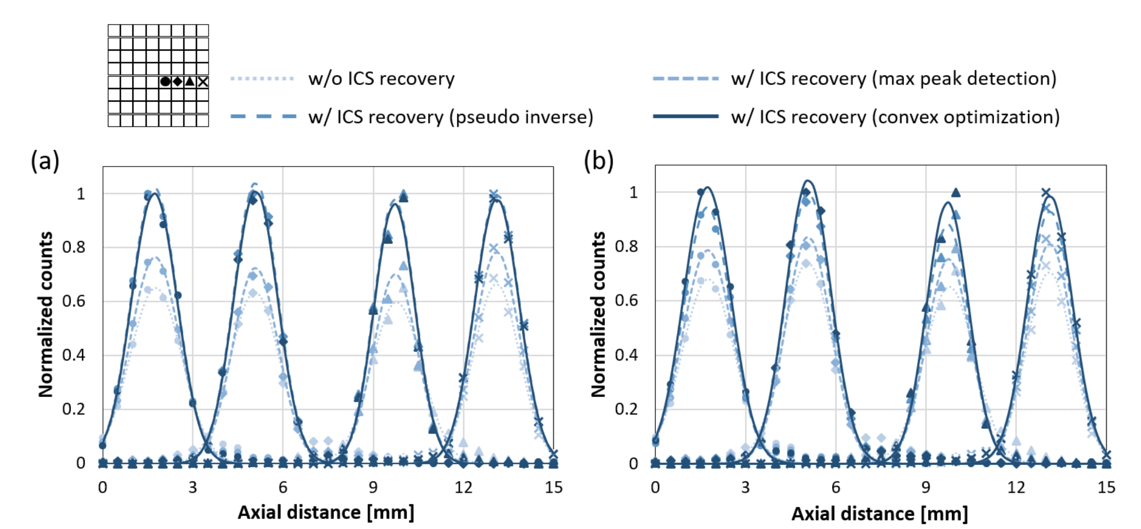

Figure 8. The intrinsic resolution profiles of four crystals in the one-to-one coupling detector with (a) the individual readout scheme and (b) the RC sum readout scheme.

Table 4. The intrinsic resolutions of the one-to-one coupling detector.

Signal readout scheme	Event identification method	FWHM (mm)	FWTM (mm)
Individual	Not applied	1.95	3.56
	Max peak detection	1.80	3.29
	Pseudoinverse	1.72	3.13
	Convex optimization	1.72	3.14
RC sum	Not applied	1.95	3.56
	Max peak detection	1.82	3.32
	Pseudoinverse	1.77	3.22
	Convex optimization	1.78	3.24

figure 8, which were normalized with respect to the maximum count in each crystal position. Both the individual and RC sum signal readout schemes were investigated. The intrinsic resolutions were averaged over four crystal positions and are reported in table 4.

After recovering the ICS events, the count profiles were sharpened with increased peak values, as shown in figure 8. When the events were identified with the proposed methods, we observed nearly a 1.5-fold increase in the count profile compared to the case without ICS recovery. The maximum peak detection method showed a 1.14-fold increase in the count profile peak values. Moreover, noting the bottom parts of the count profiles, the profiles were narrowed after ICS recovery using the proposed ICS event identifications. The average intrinsic resolutions in FWHM and FWTM for the one-to-one detector with the individual readout were 1.95 and 3.56 mm without ICS recovery, respectively. These values improved to 1.72 and 3.14 mm after recovering the ICS events identified by the convex optimization method, respectively. By recovering the ICS events, we observed an improvement in the intrinsic resolution and came closer to the ideal detector intrinsic resolution of 1.5 mm.

When detector signals were multiplexed with the RC sum scheme, the count profile intensity increase was not as remarkable as the case without signal multiplexing (figure 8(b)). However, the proposed methods showed an improvement in the intrinsic resolutions. The average intrinsic resolutions in the FWHM and FWTM were improved to 1.78 and 3.24 mm, respectively, with ICS identification using the convex optimization method.

3.2.2. Light-sharing design

The light-sharing detector was also used for experimental evaluation with the same procedure as the one-to-one coupling detector. Since the maximum peak detection method was not applicable, the pseudoinverse and convex optimization methods were used for ICS event identification. Events with and without ICS recovery are shown in figure 9 as normalized count profiles. The intrinsic resolutions were averaged over four crystal positions and are reported in table 5.

In the individual signal readout, we observed a 1.44-fold count profile intensity increase after recovering the ICS events, which were identified using the convex optimization method, as shown in figure 9(a). The average intrinsic resolutions in the FWHM and FWTM for the light-sharing detector with 1:1 signal multiplexing are 2.25 and 4.10 mm without ICS recovery, respectively. These values improved to 1.83 and 3.34 mm after recov-

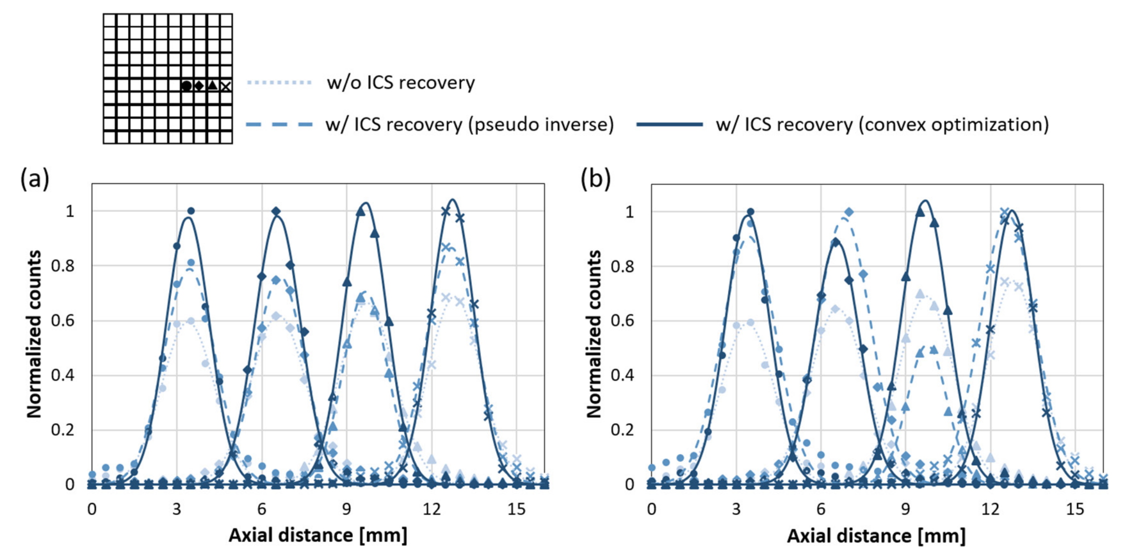

Figure 9. The intrinsic resolution profiles of four crystals in the light-sharing detector with (a) the individual readout scheme and (b) the RC sum readout scheme.

Table 5. The intrinsic resolutions of the light-sharing detector.

Signal readout scheme	Event identification method	FWHM (mm)	FWTM (mm)
Individual	Not applied	2.25	4.10
	Pseudoinverse	2.06	3.75
	Convex optimization	1.83	3.34
RC sum	Not applied	2.25	4.10
	Pseudoinverse	2.12	3.86
	Convex optimization	1.88	3.43

ering the ICS events identified by the convex optimization method, respectively. The ICS recovered intrinsic resolution in the light-sharing detector was better than that of the one-to-one coupling detector without ICS recovery. The pseudoinverse method did not show a remarkable improvement compared to the convex optimization method, and this result matched with the simulation results. The crystal, indicated as a diamond in figure 9, was located in the large gap of the dSiPM pixels and showed slight degradation, especially in the pseudoinverse method. However, the convex optimization method showed good results regardless of the crystal positions.

When signal multiplexing was applied using the RC sum, the count profile was distorted in case of the pseudoinverse method. This was mainly due to detector information loss after signal multiplexing. This information loss led to the mis-identification of the ICS events, especially for the crystals located in the gap between the pixels. However, the convex optimization method showed robust event identification in the light sharing detector with signal multiplexing, even though it showed slight degradation. The average intrinsic resolutions in the FWHM and FWTM were 2.25 and 4.10 mm without ICS recovery and improved to 1.88 and 3.43 mm after recovering the ICS events identified with the convex optimization method, respectively.

4. Discussion

In this study, we developed a new approach to identify ICS events in a PET detector by considering detector observation as a linear problem ($\boldsymbol{y} = \boldsymbol{A}\boldsymbol{x}$). The linear problem was modeled based on the observation ($\boldsymbol{y}$) and detector and event characteristics ($\boldsymbol{A}$ and $\boldsymbol{x}$). We suggested two methods to find a solution to the linear problem. The first was to calculate the pseudoinverse matrix and the second was to solve the convex constrained optimization problem. Both methods have pros and cons. The pseudoinverse method is simple and fast, but it can yield negative entries in the energy ratio vector $\boldsymbol{x}$, which will lead to a false estimation in identifying the interaction positions and energies. The convex optimization method yields a highly accurate energy ratio vector $\boldsymbol{x}$ with the given constraints, but it requires quite a long computation time. On the other hand, the proposed algorithm has advantages in that it has no dependency on the system or detector geometries.

Based on the simulation study, we investigated the performance of the ICS identification methods. The proposed methods show better performance compared to the conventional maximum peak detection approach typically used in one-to-one coupling designs. From these results, we can see that the ICS event positions cannot be discriminated correctly by locating the maximum peak positions in the integrated detector responses. Signal multiplexing leads to imprecise detector response information, and the ICS identification performance degrades significantly while using the maximum peak and pseudoinverse method. However, the proposed convex optimization method showed a reasonably good ICS identification rate and consistent energy linearity, even after signal multiplexing.

The proposed convex optimization method is also applicable to light-sharing detectors. We achieved an ICS identification rate of 0.94 with the light-sharing detector consisting of a 10×10 crystal array coupled to 8×8 pixels. The energy linearity of the convex optimization method was consistent with the light-sharing designs. The slope of the fitted energy curve was not 1, but it can be post-calibrated based on the simulation data. The proposed identification method is applicable to the light-sharing detector, even after signal multiplexing. Identifying the ICS events was challenging, with crystal-to-sensor coupling ratios larger than 1.5:1.

As an experimental study, we performed intrinsic spatial resolution measurements for the one-to-one and light-sharing detectors. After recovering ICS events into the first interaction position using the proportional method, we experimentally showed that the intrinsic resolution improved after recovering the ICS events. In the one-to-one coupling design with the individual signal readout, we observed a 12.3% resolution improvement in the FWHM and 12.6% in the FWTM. Moreover, in the light-sharing design with an individual signal readout, we observed a 19.1% resolution improvement in the FWHM and 19.3% in the FWTM. The light-sharing detector showed a resolution improvement of 17.8% in the FWHM even after signal multiplexing. The intrinsic resolution of the detector is a factor that determines the spatial resolution of the PET system. Based on these results, we expect to achieve a better spatial resolution by identifying the ICS events using the convex optimization method and recovering the first interaction positions.

5. Summary and conclusion

We have proposed a new method to classify and identify ICS events in a PET detector. The proposed method successfully identifies ICS events with high accuracy, even in PET detectors with light-sharing designs. The identified ICS events were recovered into the first interaction position, and an improved intrinsic resolution was observed after ICS recovery. The proposed method can be applied to PET detectors or system designs that consist of light-sharing detector design, even with moderate signal multiplexing.

Acknowledgments

This work was supported by grants from the National Research Foundation of Korea (NRF) funded by the Korean Ministry of Science, ICT and Future Planning (grant no. NRF-2014M3C7034000 and NRF-2016R1A2B3014645) and by a grant from the Korea Health Technology R&D Project through the Korea Health Industry Development Institute (KHIDI) funded by the Ministry of Health and Welfare, Republic of Korea (grant no. HI14C1135).

ORCID iDs

Jae Sung Lee https://orcid.org/0000-0001-7623-053X

References

Ahn B-C 2017 Nuclear medicine in the era of precision medicine *Nucl. Med. Mol. Imaging* **51** 99–100

Alessio A M, Kinahan P E and Lewellen T K 2006 Modeling and incorporation of system response functions in 3D whole body PET *IEEE Trans. Med. Imaging* **25** 828–37

Comanor K, Virador P and Moses W 1996 Algorithms to identify detector Compton scatter in PET modules *IEEE Trans. Nucl. Sci.* **43** 2213–8

Grant M and Boyd S 2011 CVX Research, Inc. CVX: Matlab software for disciplined convex programming, version 2.0 (http://cvxr.com/cvx/)

Gross-Weege N, Schug D, Hallen P and Schulz V 2016 Maximum likelihood positioning algorithm for high-resolution PET scanners *Med. Phys.* **43** 3049–61

Jan S *et al* 2004 GATE: a simulation toolkit for PET and SPECT *Phys. Med. Biol.* **49** 4543–61

Jan S *et al* 2011 GATE V6: a major enhancement of the GATE simulation platform enabling modelling of CT and radiotherapy *Phys. Med. Biol.* **56** 881–901

Kim J S 2016 Combination radioimmunotherapy approaches and quantification of immuno-PET *Nucl. Med. Mol. Imaging* **50** 104–11

Lage E, Parot V, Moore S C, Sitek A, Udias J M, Dave S R, Park M A, Vaquero J J and Herraiz J L 2015 Recovery and normalization of triple coincidences in PET *Med. Phys.* **42** 1398–410

Lee M S and Lee J S 2015 Depth-of-interaction measurement in a single-layer crystal array with a single-ended readout using digital silicon photomultiplier *Phys. Med. Biol.* **60** 6495–514

Lee M S, Kim K Y, Ko G B and Lee J S 2017 Prototype pre-clinical PET scanner with depth-of-interaction measurements using single-layer crystal array and single-ended readout *Phys. Med. Biol.* **62** 3983–96

Levin A and Moisan C 1996 A more physical approach to model the surface treatment of scintillation counters and its implementation into DETECT *IEEE Nuclear Science Symp. Conf. Record* vol 2 pp 702–6

Levin C S and Zaidi H 2007 Current trends in preclinical PET system design *PET Clin.* **2** 125–60

Ling T, Lewellen T K and Miyaoka R S 2007 Depth of interaction decoding of a continuous crystal detector module *Phys. Med. Biol.* **52** 2213–28

Panin V Y, Kehren F, Michel C and Casey M 2006 Fully 3D PET reconstruction with system matrix derived from point source measurements *IEEE Trans. Med. Imaging* **25** 907–21

PDPC-TEK User Manual 2014 *Philips Digital Photon Counting*

Phelps M E 2000 Positron emission tomography provides molecular imaging of biological processes *Proc. Natl Acad. Sci. USA* **97** 9226–33

Pratx G and Levin C S 2009 Bayesian reconstruction of photon interaction sequences for high-resolution PET detectors *Phys. Med. Biol.* **54** 5073–94

Rafecas M, Böning G, Pichler B, Lorenz E, Schwaiger M and Ziegler S 2003 Inter-crystal scatter in a dual layer, high resolution LSO-APD positron emission tomograph *Phys. Med. Biol.* **48** 821–48

Rahmim A, Qi J and Sossi V 2013 Resolution modeling in PET imaging: theory, practice, benefits, and pitfalls *Med. Phys.* **40** 064301

Roncali E and Cherry S R 2011 Application of silicon photomultipliers to positron emission tomography *Ann. Biomed. Eng.* **39** 1358–77

Shao Y, Cherry S R, Siegel S and Silverman R W 1996 A study of inter-crystal scatter in small scintillator arrays designed for high resolution PET imaging *IEEE Trans. Nucl. Sci.* **43** 1938–44

Surti S and Karp J S 2018 Impact of event positioning algorithm on performance of a whole-body PET scanner using one-to-one coupled detectors *Phys. Med. Biol.* **63** 055008